ROBOT SERVICER INTERACTION WITH A SATELLITE DURING CAPTURE

Justin Brannan[1], Nicholas Scott[2], Craig Carignan[3]

[1]*Millennium Engineering and Integration Company, Arlington, Virginia, USA, E-mail: jbrannan@meicompany.com*
[2]*Jackson and Tull, Greenbelt, Maryland, USA, E-mail: nicholas.a.scott@nasa.gov*
[3]*Space Systems Laboratory, University of Maryland, College Park, Maryland, USA, E-mail: craigc@ssl.umd.edu*

ABSTRACT

On-orbit failures that typically lead to satellite end-of-life may soon be fixed and returned to operation using robotic servicing platforms. To demonstrate the feasibility of robotic servicing, it is necessary to develop a high-fidelity ground simulation of how a servicer spacecraft and client satellite interact. This can be achieved by using robotic hardware-in-the-loop simulation platforms that physically interact to generate realistic contact loads that feed into a dynamic model of the on-orbit system.

This paper presents two main improvements to previous work discussed in [1]: (a) pre-contact initial motion of the client satellite system; (b) inclusion of flexible-body dynamics into the satellite simulation. First, the ground simulation hardware and controllers used to achieve the simulation are described. Then force-motion results from the higher fidelity interaction during grapple are discussed for a range of parameters and initial conditions.

1 INTRODUCTION

Robotic on-orbit servicing has the potential to drastically reduce the lifecycle cost of future missions and increase both the reliability and safety of access to space [2, 3, 4]. The mission scenario used during this research includes a free-flying servicing vehicle with robotic arms which must rendezvous, grapple, service and release a client satellite. In pursuit of such a mission, various on-orbit demonstrations such as Japan's National Space Development Agency (JAXA) Engineering Test Satellite No. 7 (ETS-VII) [5] and the United States Defense Advanced Research Projects Agency (DARPA) Orbital Express Mission [6] have focused on proof-of-concept experiments to demonstrate the technologies needed.

A critical phase of the servicing mission is the rendezvous and grapple sequence between servicing vehicle and client satellite. Both the strict time-constraint to achieve grapple and the risk of excess energy transfer during contact could result in failure to achieve grapple. The use of software-only simulations can assist with a part of this technology development but is limited by its ability to accurately replicate contact dynamics between the two spacecraft. Commonly used hardware-based simulation platforms can further develop these maneuvers, however the added viscous forces during neutral buoyancy simulations, limited time and imperfections introduced with a zero-gravity parabolic flight, and lack of out-of-plane dynamics on an air bearing table limit the utility of these platforms when studying the contact dynamics.

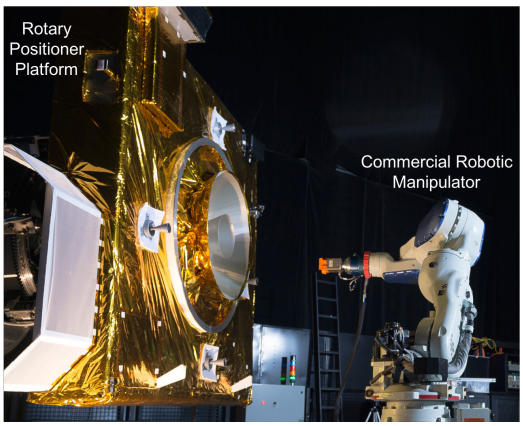

Figure 1: Ground-based robotic simulation platform including rotary positioner which simulates the client satellite motion and commercial robot that simulates the servicer robot arm.

Robotics-based hardware-in-the-loop (HITL) simulators, such as the platform seen in Fig. 1, can effectively implement active gravity compensation and can accommodate complex systems that require unconstrained motion within the robot workspaces. Many government agencies, academic institutions, and industrial partners are developing such platforms to emulate the six degree-of-freedom rigid-body motion of spacecraft in support of on-orbit satellite servicing missions, where a free-floating servicing

spacecraft will demonstrate various robotic operations to extend the life of satellites on-orbit [7, 8, 9, 10, 11, 12, 13, 14, 15, 16]. The work described here seeks to increase the fidelity of the interaction through improved modeling and more realistic rendezvous conditions.

An introduction to the simulation platforms used in this research will be given in Section 2, including a detailed explanation of the robotic servicer and client dynamics. Section 3 introduces the test setup details and results to support the two main contributions of this paper. A discussion and some concluding remarks will be given in Section 4.

2 SIMULATOR OVERVIEW

This research utilizes a ground-based robotic simulation platform at the NASA Goddard Space Flight Center to study the interaction dynamics between a robotic servicer and client satellite. The testbed, shown in Fig. 1, features a commercial robotic manipulator which plays the role of the servicer's robotic arm and a mockup of a client satellite attached to a rotary positioner platform, which is capable of 360° of rotation and serves as a satellite simulator. A more detailed depiction of the relationship between the ground-based HITL simulation and simulated on-orbit dynamics is shown in Fig. 2, and is further explained in the following sections.

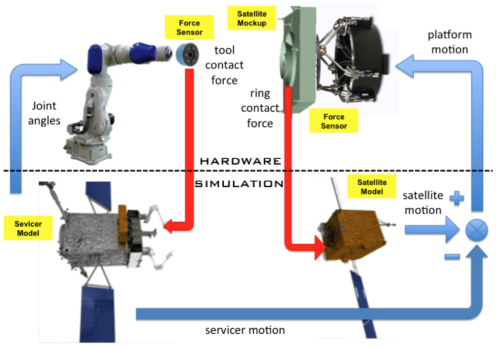

Figure 2: On-orbit servicer and client satellite dynamics being simulated by ground-based HWIL robotic platforms.

2.1 Simulation of Servicer Dynamics

The commercial robotic manipulator used in this research is programmed to follow an automated grapple trajectory including visual feedback from a camera attached to its end-effector, as is portrayed in the block diagram in Fig. 3. An external vision system is used to feed back the client spacecraft position (C) relative to the servicer spacecraft (S), ${}^{S}r_{C}$, which is used with the desired grapple trajectory, x_{in}, and measured position of the robot, x_{meas}, to produce the commanded trajectory of the robot end-effector, x_{cmd}.

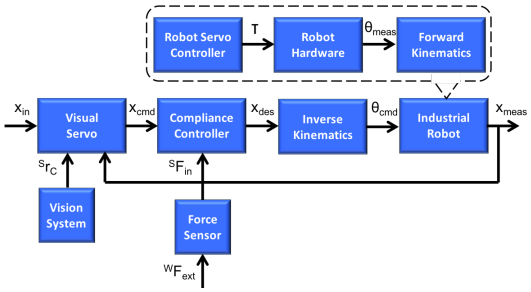

Figure 3: Block diagram of the force and position loops behind the commercial manipulator simulation of the robotic servicer during grapple.

The commanded trajectory, along with the interaction forces sensed by the force sensor on the commercial robot are fed into the compliance controller which reacts according to (1), to effectively manage the relationship between force and tool tip velocity once initial contact is measured with the Marman ring. This effect can be tuned by using a 6x6 matrix of desired mass (M), damping (B), and stiffness (K) gains to achieve the desired performance specifications based on the environment of interest, as previously reported in [1].

$$ {}^{S}F_{in} = M\left(\ddot{x}_d - \ddot{x}\right) + B\left(\dot{x}_d - \dot{x}\right) + K\left(x - x_d\right) \quad (1) $$

Note that the simulation does not currently account for servicer hub motion or the motion due to the coupled interaction between the servicer robotic manipulator and the servicer hub. Ultimately, this affects the interaction forces experienced by the client satellite which might not accurately represent what will be experienced on orbit. A flight-like representation of the servicer dynamics has been examined using commercial dynamics simulation software (ADAMS), which has indicated significant servicer hub motion yet negligible arm/servicer interaction. For this reason, it is planned to include the servicer hub dynamics in future testing.

2.2 Simulation of Client Dynamics

A more detailed diagram of the client satellite motion, as simulated by the rotary positioner platform is shown in Fig. 4, where the sensed forces caused by contact with the robotic servicer are recorded by the sensor attached to the mock satellite. This force profile is input to the satellite system dynamics, and the resulting desired client satellite motion is output to the robot tracking controller. The robot inverse kinematics and robot servo controller are then used to compute the torques that actually drive the rotary positioner platform hardware, and the robot forward kinematics model outputs the realized robot motion, which is what is physically seen by the resulting client satellite mockup motion.

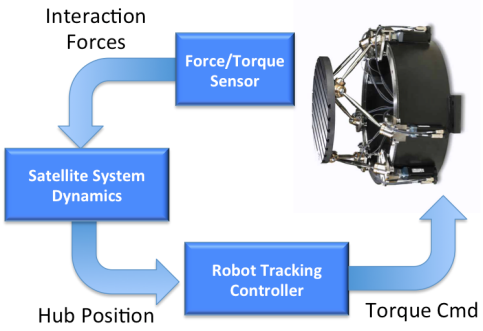

Figure 4: Block diagram of the rotary positioner simulated client satellite response to contact with the robotic servicer during grapple.

The equations of motion for a client satellite reacting to interaction forces from a robotic servicing vehicle are given in (2), where more details about the inertia matrix, M_{system}, and velocity terms, Q_{system} can be found in [17, 18]. Key assumptions from this derivation include: the client satellite has a single rigid-body satellite hub with two symmetrically-located flexible appendages; each appendage can be accurately represented by a Euler-Bernoulli beam; the dominant response of the system can be captured using only the first few modes; and each appendage can be approximated as having a single flexible degree-of-freedom.

$$\left[M_{system}\right]\left[\ddot{\bar{x}}\right] = \left[Q_{system}\right] + \left[\bar{u}_{input}\right] \tag{2}$$

$$M_{system} = \begin{bmatrix} M_{RR} & M_{R\theta} & \bar{S}_1 & \bar{S}_2 \\ M_{R\theta}{}^T & M_{\theta\theta} & \bar{I}_{\theta f1} & \bar{I}_{\theta f2} \\ \bar{S}_1{}^T & \bar{I}_{\theta f1}{}^T & m_{ff1} & 0_{nxn} \\ \bar{S}_2{}^T & \bar{I}_{\theta f2}{}^T & 0_{nxn} & m_{ff2} \end{bmatrix} \tag{3}$$

Let $\left[\bar{x}^T\right] = \left[R^T, \theta^T, q_f^T\right]$ represent the combined flexible-body state of the satellite in body frame, where R is the rigid-body position of the hub, θ is the rigid-body orientation of the hub, and q_f is the modal position of the satellite appendages. The external input profile is represented in the satellite body frame by $\left[\bar{u}_{input}^T\right] = \left[\bar{F}_{ext}^T, \bar{T}_{ext}^T, \bar{Q}_{ext}^T\right]$, which includes the rigid-body and modal forces ($\bar{F}_{ext}$, $\bar{Q}_{ext}$) as well as the applied torques ($\bar{T}_{ext}$) experienced from the initial contact of a servicer arm.

This interaction with the servicer robotic arm causes both translation and rotation of the client satellite, as indicated by the red arrows in Fig 5. The single DOF of each appendage is about the z-axis such that the appendage oscillations stay in the y-z plane. However, the satellite hub motion is free to move in any direction.

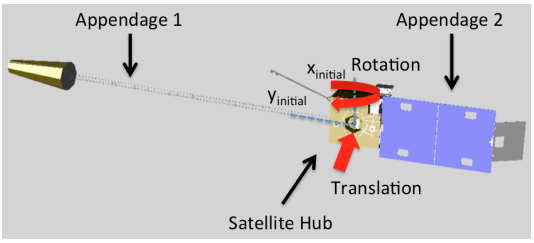

Figure 5: Example client satellite rigid-body hub and flexible-body appendages including resultant translation and rotation during grapple.

3 TEST RESULTS

Previous research has focused on the capture of a stationary rigid-body client satellite by a robotic arm mounted to the servicing vehicle [1]. This baseline test case includes the robotic capture of a 2000 kg rigid-body client satellite, according to the details explained in Section 2.

Typical force/torque profiles are shown in Fig. 6. The initial contact occurs just prior to 193 seconds, where the z-direction is normal to the contact surface. The force in the y-direction at 194.5 seconds shows the lateral forces of the gripper closing on the Marman ring, where the last stage of the grapple maneuver is seen in Fig. 7. At 196 seconds, the start of the deceleration phase is evident by the spikes in force and torque. The following oscillations occur during the continued rate null maneuver as the robot arm reduces the client satellite velocity to zero.

The expected resulting motion, shown in Fig. 8, includes both translation in the direction of initial

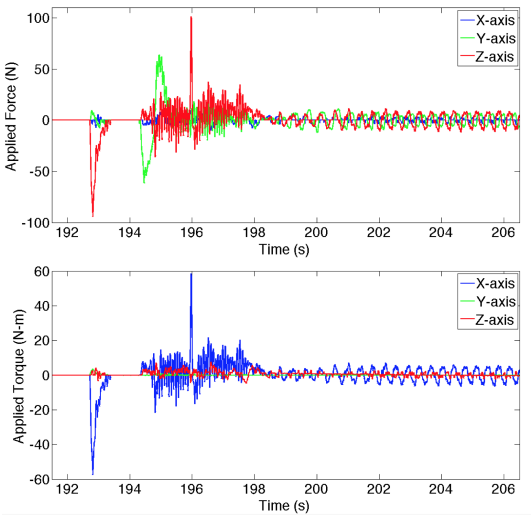

Figure 6: Example contact loads during baseline grapple maneuver with a 2000 kg client satellite.

Figure 7: Overhead view of a grapple maneuver, showing the robotic manipulator with attached gripper tool before contact with the Marman ring.

contact (z-axis) and rotation due to the resolved moment about the client satellite's body (S) frame, since there is an initial offset between the contact location on the Marman ring and the client satellite center of mass.

3.1 Addition of Initial Velocity

Two features will be added to this baseline test case to improve the fidelity of the on-orbit dynamics simulation. First, initial motion of the client satellite is introduced which will lead to larger forces and torques as the satellite's momentum is absorbed by the stationary servicer system.

For this initial study, the rotary positioner platform seen in Fig. 1 is driven to follow a single-axis rotation about the satellite (S) frame, seen in Fig. 9. During this maneuver, the motion of a 1000 kg client satellite is simulated, with center

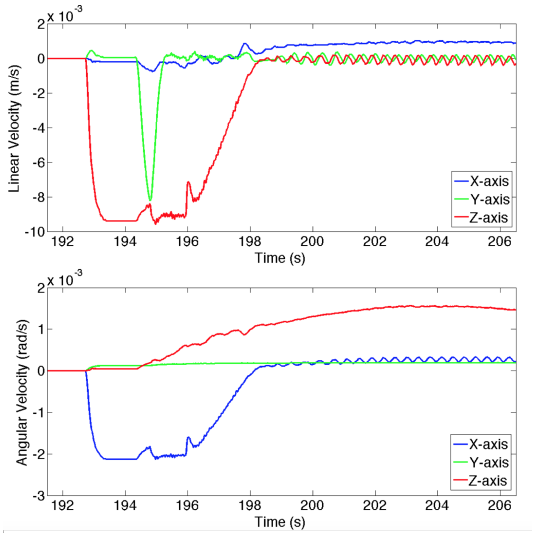

Figure 8: Resulting linear and angular velocity of a 2000 kg rigid-body client satellite during baseline grapple maneuver.

of mass 1 meter behind the center of the marman ring, and primary axes of inertia approximately (3500, 1000, 3500) kg-m^2. Three sets of initial conditions are introduced: a control group with no rotational rate; an initial angular velocity of 0.25 deg/s; and an initial angular velocity of 0.33 deg/s.

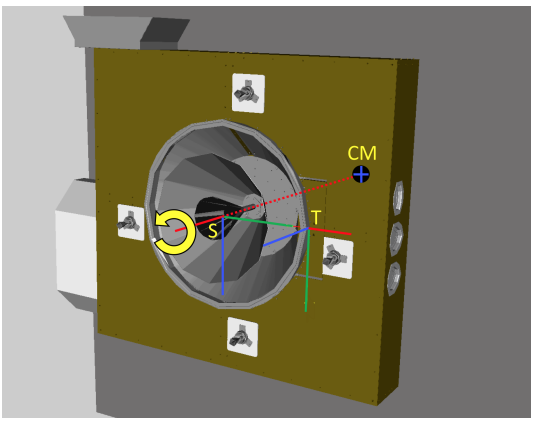

Figure 9: Visualization of the client mockup satellite (S) and tool (T) frames.

After initial contact, which occurs at the origin of the tool frame (T) in Fig. 9, the robotic manipulator arm is programmed to remove momentum from the client satellite until the client vehicle's motion comes to a halt. This can be seen for the 0.33 deg/s initial condition case in Figs. 10 and 11, where the linear and rotational velocities decrease from initial contact until the end of the grapple maneuver, at approximately 1943 seconds. Note that the velocity data is represented in satellite (S)

frame whereas the plot of contact loads are represented in tool (T) frame.

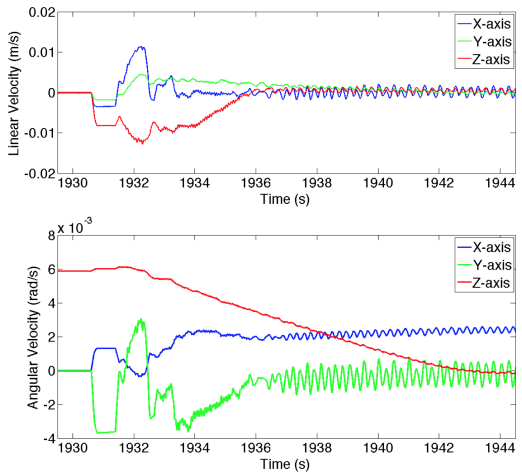

Figure 10: Resulting linear and angular velocity of a 1000 kg rigid-body client satellite during grapple with an initial condition of 0.33 deg/s.

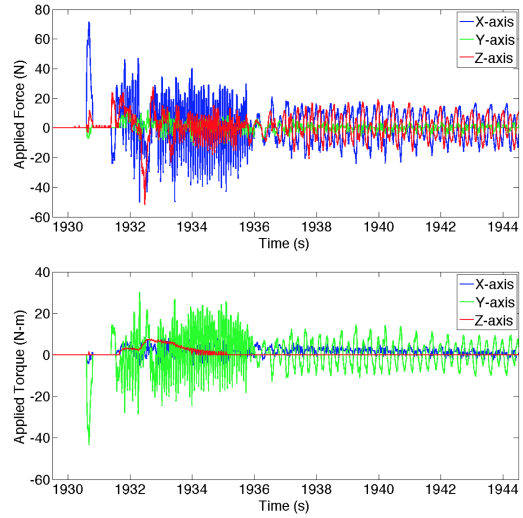

Figure 11: Example contact loads during grapple maneuver with a 1000 kg rigid-body client satellite, and initial condition of 0.33 deg/s.

The final results are summarized in Table 1, where separate integrations were performed for each axis from the time of initial contact through the completion of the grapple maneuver, such that the force impulse about the x-axis for the 0.33 deg/s initial condition is -1.2 N-s.

As expected, adding initial angular momentum in the form of an initial rotation about the z-axis of the satellite frame results in larger torques experienced by the client satellite, about the given axis.

Table 1: Impulse calculations for initial condition test cases of a 1000 kg rigid-body client satellite.

$\omega_{z_{init}}$ (°/s)	Force Impulse (N-s)			Torque Impulse (N-m-s)		
0	0.2	0.3	0.1	0.2	-0.1	0.2
0.25	-1.0	2.2	1.6	14.5	-2.6	8.1
0.33	-1.2	2.9	2.2	22.2	-3.4	11.8

This is evident by comparing the torque impulse of 0.2 N-m-s when the client satellite has no initial condition, to 14.5 N-m-s for a 0.25°/s initial angular velocity, and 22.2 N-m-s for an initial rotational velocity of 0.33°/s. In this case, a 33% increase in initial velocity resulted in a 50% increase in torque impulse.

Note that the asymmetry of the client satellite mass properties results in significantly different motion in each direction. For example, the client satellite inertia about the y-axis is three times smaller than the other two axes, which correlates with the factor of three when comparing the y and z-axis torque impulse values for the 0.25 and 0.33 deg/s initial condition cases.

Furthermore, preliminary rigid-body capture tests have indicated that misalignment of the robotic gripper could produce a large torque as the gripper closes. This is evident around 1932.5 seconds in Fig. 11 and seems to affect the y and z-axis torque values both due to the offset between the contact point and client satellite center of mass, and expected misalignment of the gripper. Although the force impulse data for the three input cases are less conclusive than the torque impulse data trends, a noise floor of 0.3 N-s of force impulse can be established, and the same general trend exists, where larger initial conditions result in larger forces being experienced by the client satellite.

3.2 Addition of Flexible-body Dynamics

The second study entails adding client satellite flexible-body dynamics to the HITL simulation, to more accurately capture how the client reacts to the interaction with the robotic servicer. The motion profile is expected to change significantly with the addition of this flexible-body motion.

For these tests, two symmetrically placed appendages are introduced, to represent a generic class of client satellites with booms, antennas, and/or solar panels. Unlike the grapple maneuvers from the first study, no external vision package is required since no initial conditions are present,

so the robotic manipulator arm uses dead reckoning to simply plunge forward at 1 cm/s until contact, and continues forward until grasp is achieved. Three sets of client satellite mass parameters are used to compare the rigid-body response against that of a flexible-body satellite, due to the same interaction with a servicer robot arm.

The interaction forces between the robotic manipulator arm and a 2000 kg flexible-body client satellite are shown in Fig. 12. Although comparable to the rigid-body example given in Fig. 6 at first glance, the broader spectrum of oscillations are attributed to the addition of these flexible appendages.

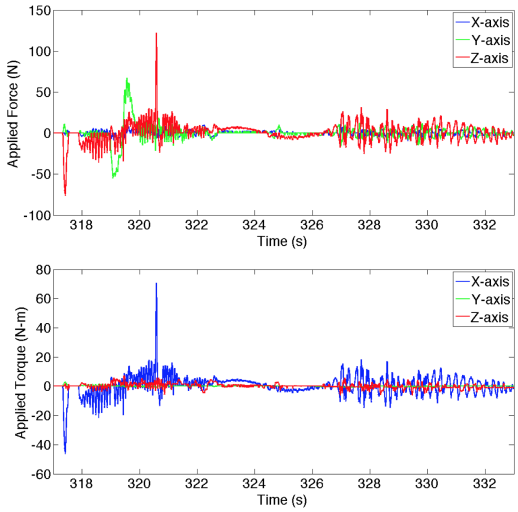

Figure 12: Example contact loads during grapple maneuver with a 2000 kg flexible-body satellite.

By introducing impulse calculations, it is possible to better quantify the differences between these two sets of data. Similar to the approach taken in Section 3.1, the impulse is found by integrating the force and torque plots. However, for this study, the integration occurs only during the initial contact, to focus on the momentum transferred prior to arresting the client satellite motion.

Table 2 summarizes the root mean squared values of the impulse values for six sets of mass properties, including both rigid-body and flexible-body test cases. For example, the integration of force from time 317 until just before 319 seconds, as seen in Fig. 12, correlates to the resulting data point of 21.82 N-s.

As expected, there is a proportional relationship between the satellite hub mass and the force and torque impulse values, evident by the increase

Table 2: Impulse calculations to compare rigid-body (no appendage mass) and flexible-body client satellite responses to a grapple maneuver.

	Satellite Mass (kg)	App. Mass (kg)	Force Impulse (N-s)	Torque Impulse (N-m-s)
1	1000	-	9.38	5.66
2	1000	25	11.85	7.19
3	2000	-	18.97	11.49
4	2000	50	21.82	13.18
5	4000	-	37.42	22.66
6	4000	100	38.63	23.37

in force impulse measurement when comparing any two successive mass cases, either for the rigid-body (no appendage mass) or the simulation of a flexible-body client satellite. For example, the force impulse increases proportionally to the mass, from 9.38 N-s to 18.97 N-s, for a 1000 kg and 2000 kg rigid-body satellite, respectively.

When comparing the impulse for a rigid-body versus flexible-body spacecraft, it is evident that the introduction of flexible-body dynamics generally increases the force/torque impulse. Part of this can be attributed to the additional mass compared to the rigid case, as the mass of each appendage increases with increasing hub mass to maintain a hub-to-appendage mass ratio of 40:1 for each test case. In the case of the 2000 kg satellite, the force impulse showed an increase from 18.97 Ns to 21.82 N-s, approximately a 15% increase, with the introduction of two 50 kg flexible-body appendages, whereas the mass only increased by 5%. Increasing each appendage mass to 100 kg resulted in the same trend, increasing the force impulse by 3 N-s and torque impulse by 1.5 N-m-s

In addition to the interaction forces, the linear and angular velocity of the resulting motion of the flexible-body client satellite are given in Fig. 13, where the initial contact from the robotic manipulator arm produces a maximum linear velocity on the order of 1 cm/s and angular velocity on the order of 0.01 rad/s (0.7 deg/s).

The oscillations resulting from the addition of flexible appendages are seen in the velocity plots in Fig. 13, which were not observed previously in Fig. 8. It is evident that additional energy is being stored in the flexible appendages, since they continue to oscillate after the robotic manipulator has successfully acquired the client satellite, at approximately 324 seconds. Although the

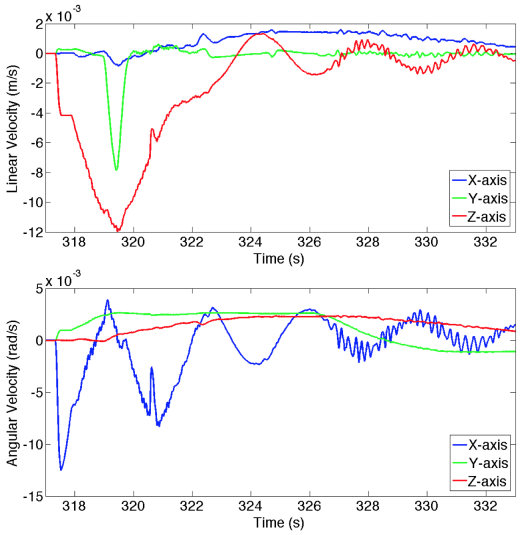

Figure 13: Resulting linear and angular velocity of a 2000 kg flexible-body client satellite during grapple, showing the 0.3 Hz modal frequency.

magnitude of these oscillations are only 2 mm/s and 0.3 deg/s, it is plausible that the introduction of larger appendages, smaller satellite hub mass, or more asymmetrical appendages could result in more contribution to the translational motion of the client satellite.

4 CONCLUSION

Two major contributions to the current ground-based robotic HITL platforms have been introduced to more accurately simulate how a robotic servicer and client satellite will interact during a nominal on-orbit mission.

An initial study of the momentum transfer during autonomous grapple maneuvers has been introduced to identify how the addition of client satellite initial conditions contribute to the resulting dynamics of the client-servicer system. Force/torque plots have been compared against a baseline mass case, and the resulting velocity plots characterize the motion of the HITL simulation platforms.

It was found that adding flexible-body dynamics to a rigid-body spacecraft model can lead to significant contributions to the overall system motion. This is particularly important if the servicer or client spacecraft feature asymmetric appendages of significant mass compared to the satellite hub.

Proposed future work includes testing larger initial conditions to further characterize the correlation between initial conditions, force impulse, and momentum transfer between the two vehicles. A focused study on the servicer dynamics is also warranted, which includes adding this motion to the rotary positioning platform to simulate the relative motion of the two spacecraft, and introducing the robotic servicing arm and servicer spacecraft motion. Related work might include a more thorough investigation to compare whether or not the flexible-body appendages can survive the loading profile during grapple and the ensuing servicing operations on orbit. Impulse-based characterizations should also be applied to a more flight-like scenario, to analyze whether or not the robotic arm will be capable of producing the interaction forces and torques to successfully capture and arrest the motion of a given client satellite. Finally, a direct comparison of the higher-fidelity HITL simulations against on-orbit data would enable an end-to-end validation of the techniques presented in this research to better prepare for future satellite servicing endeavors.

Acknowledgement

This work was performed as part of the NASA Goddard Space Flight Center Satellite Servicing Project Division's technology development efforts in support of robotic servicing. We would like to acknowledge the entire team in the Robotic Development Test Facility for making this work possible.

References

[1] Carignan C, Scott N and Roderick S (2014) Hardware-in-the-Loop Simulation of Satellite Capture in a Ground-based Robotic Testbed. In: *Proc. of the International Symposium on Artificial Intelligence, Robotics and Automation in Space (i-SAIRAS)*, Montreal, Canada.

[2] Ellery A, Kreisel J and Sommer B (2008) The case for robotic on-orbit servicing of spacecraft: Spacecraft reliability is a myth. In: *Acta Astronautica*, 63:pp.632–648.

[3] Tafazoli M (2009) A study of on-orbit spacecraft failures. In: *Acta Astronautica*, 64:pp.195–205.

[4] Hollander S (2000) Autonomous Space Robotics: Enabling Technologies for Advanced Space Platforms. In: *AIAA Space 2000 Conference and Exposition*, AIAA 2000-5079, AIAA, Long Beach, CA.

[5] Yoshida K (2003) Engineering Test Satellite VII Flight Experiments for Space Robot Dynamics and Control: Theories on Laboratory Test Beds Ten Years Ago, Now in Orbit. In: *The International Journal of Robotics Research*, 22(5):pp.321–335.

[6] Leinz MR, Chen CT, Scott P, Gaumer W, Sabasteanski P and Beaven M (2008) Modeling, simulation, testing, and verification of the Orbital Express Autonomous Rendezvous and Capture Sensor System (ARCSS). In: *Society of Photo-Optical Instrumentation Engineers (SPIE) Conference Series*, volume 6958. doi:10.1117/12.779599.

[7] Yoshida K, Nakanishi H, Ueno H, Inaba N, Nishimaki T and Oda M (2004) Dynamics, Control and Impedance Matching for Robotic Capture of a Non-cooperative Satellite. In: *Advanced Robotics*, 18(2):pp.175–198.

[8] Xu W, Liang B, Xu Y, Li C and Qiang W (2007) A Ground Experiment System of Free-floating Robot For Capturing Space Target. In: *Journal of Intelligent and Robotic systems*, 48(2):pp.187–208.

[9] Kaiser C, Sjoberg F, Delcura J and Eilertsen B (2008) SMART-OLEV - An orbital life extension vehicle for servicing commercial spacecrafts in GEO. In: *Acta Astronautica*, 63:pp.400–410.

[10] Boge T, Wimmer T, Ma O and Tzschichholz T (2010) Epos-using robotics for RvD simulation of on-orbit servicing missions. In: *AIAA Modeling and Simulation Technologies Conference*.

[11] Benninghoff H, Tzschichholz T, Boge T and Rupp T (2011) Hardware-in-the-Loop Simulation of Rendezvous and Docking Maneuvers in On-Orbit Servicing Missions. In: *Proc. of the 28th International Symposium on Space Technology and Science*, Okinawa.

[12] Boge T, Benninghoff H, Zebenay M and Rems F (2012) Using Robots for Advanced Rendezvous and Docking Simulation. In: *Proc. of the Simulation and EGSE facilities for Space Programmes*, Noordwijk.

[13] Ma O, Flores-Abad A and Boge T (2012) Use of industrial robots for hardware-in-the-loop simulation of satellite rendezvous and docking. In: *Acta Astronautica*, 81(1):pp.335–347.

[14] Flores-Abad A, Ma O, Pham K and Ulrich S (2014) A review of space robotics technologies for on-orbit servicing. In: *Progress in Aerospace Sciences*, 68:pp.1–26.

[15] Zebenay M, Boge T, Krenn R and Choukroun D (2015) Analytical and experimental stability investigation of a hardware-in-the-loop satellite docking simulator. In: *Proc. of the Institution of Mechanical Engineers, Part G: Journal of Aerospace Engineering*, 229(4):pp.666–681. doi:10.1177/0954410014539290.

[16] Artigas J, Stefano MD, Rackl W, Lampariello R, Brunner B, Betreff W, Burger R, Portes O, Giordano A, Borst C and Albu-Shaeffer A (2015) The OOS-SIM: An On-ground Simulation Facility For On-Orbit Servicing Robotic Operations. In: *IEEE 2015 International Conference on Robotics and Automation*, Seattle.

[17] Brannan JC and Carignan CR (2013) Modeling Flexible-Body Dynamics in Real-Time Robotic Systems used in Satellite Servicing Simulations. In: *AIAA Modeling and Simulation Technologies Conference*, AIAA 2013-5157, AIAA, Boston, MA.

[18] Brannan JC and Carignan CR (2017) Interaction of a Robotic Servicing Vehicle with Satellite Modes during Capture. In: *AIAA Modeling and Simulation Technologies Conference*, AIAA 2017-1555, AIAA, Grapevine, TX.